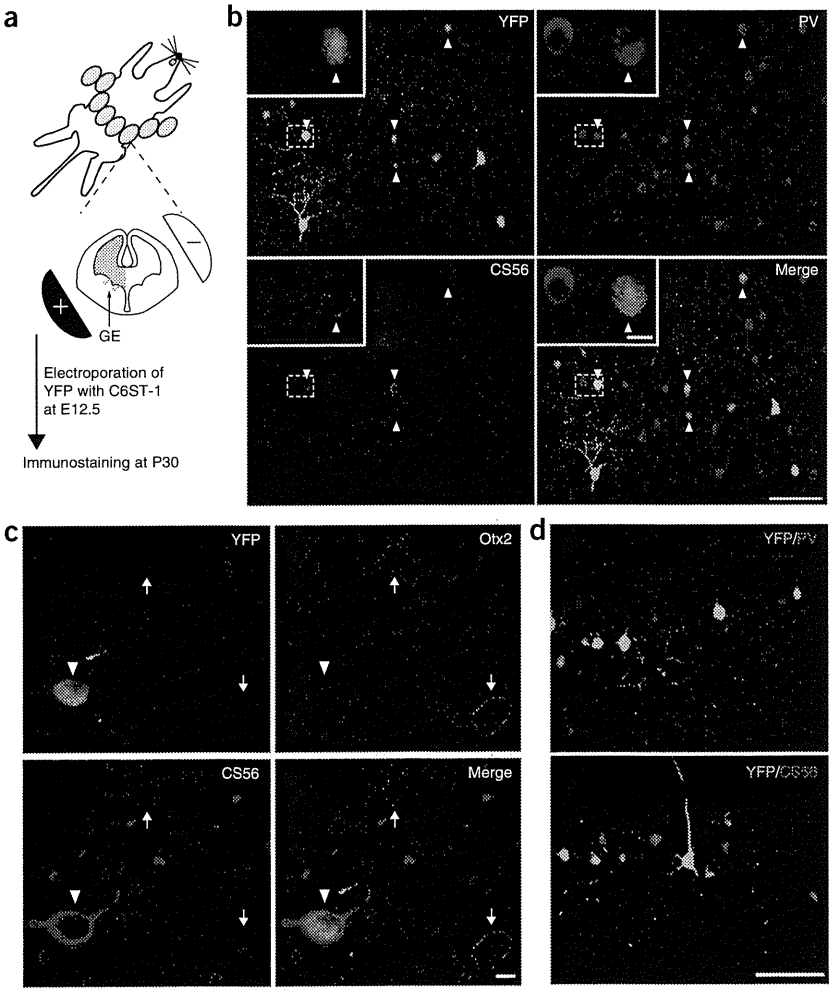

Figure 6 Overexpression of C6ST-1 in parvalbumin-expressing interneurons cell-autonomously affects PNN formation. (**a**) Experimental model for ganglionic eminence (GE)–directed electroporation. Wild-type interneurons were co-electroporated with *C6ST-1* and *YFP* at E12.5 and analyzed at P30. (**b**) CS56$^+$ PNNs were formed around co-transfected parvalbumin-expressing interneurons (arrowheads). Insets, magnification of boxed regions. Note that the transfected (right), but not the neighboring untransfected (left), parvalbumin-expressing interneurons were surrounded by CS56$^+$ PNNs. (**c**) Otx2 signal was not found in transfected parvalbumin-expressing interneurons surrounded by CS56$^+$ PNNs (arrowheads). Arrows indicate Otx2 accumulation in untransfected parvalbumin-expressing interneurons. (**d**) Overexpression of C6ST-1 in excitatory pyramidal neurons resulted in no YFP signal in parvalbumin-expressing interneurons and CS56$^+$ PNNs. Scale bars represent 100 μm (**b–d**) and 10 μm (insets in **b**).

feature of fast-spiking cells[29,30], was commonly found in both groups (**Fig. 7a**). No significant difference was found in the ratio of the last interspike interval to the second interspike interval (wild type, $n = 5$ neurons, 1.4 ± 0.15; *C6ST-1* transgenic, $n = 6$ neurons, 1.4 ± 0.18; $P > 0.7$). Furthermore, both groups showed another feature of fast-spiking cells: short-duration action potentials followed by fast afterhyperpolarizations[29,30] (**Fig. 7a**). Although no significant difference was found in the amplitude (wild type, $n = 5$ neurons, 16 ± 0.38 mV; *C6ST-1* transgenic, $n = 6$ neurons, 17 ± 0.49 mV; $P > 0.2$) or duration (wild type, $n = 5$ neurons, 26 ± 2.8 ms; *C6ST-1* transgenic, $n = 6$ neurons, 28 ± 2.9 ms; $P > 0.6$) of the afterhyperpolarization, the action potentials were significantly wider ($P < 0.009$) in *C6ST-1* transgenic mice than in wild-type mice (**Fig. 7b**). In addition, the resting membrane potential was significantly more depolarized ($P < 0.03$; **Fig. 7c**) in *C6ST-1* transgenic mice, although no difference was found in input resistance (wild type, $n = 5$ neurons, 145 ± 22.1 MΩ; *C6ST-1* transgenic, $n = 6$ neurons, 166 ± 20.7 MΩ; $P > 0.3$). Parvalbumin immunoreactivity was detected in all of the fast-spiking cells (four cells in wild-type mice and five cells in *C6ST-1* transgenic mice) in which we successfully conducted immunohistochemical examinations (**Fig. 7a**). A recent study on parvalbumin-expressing interneurons found that a shortening of spike width and a hyperpolarization of resting membrane potential proceeded in parallel with changes in the other membrane properties during postnatal development[31]. Thus, the overexpression of C6ST-1 prevented the maturation of some of the electrophysiological properties of parvalbumin-expressing interneurons.

In *C6ST-1* transgenic mice, parvalbumin-expressing interneurons may more easily initiate action potentials in response to excitatory inputs, as a result of their depolarized membrane potentials, and therefore inhibit their target cells more frequently than in wild-type mice. The shortening of spike width results in a reduction of transmitter release probability and short-term depression at the nerve terminals

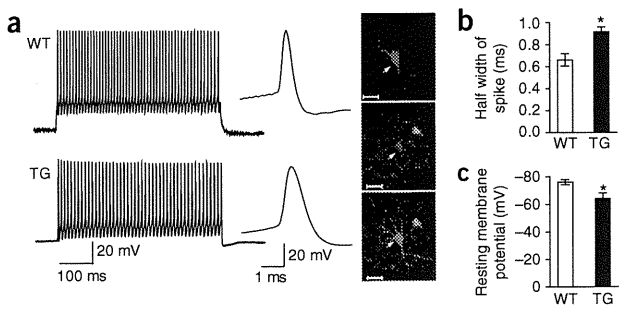

Figure 7 Overexpression of C6ST-1 prevents the maturation of the membrane properties of fast-spiking cells. (**a**) Example traces of spike discharges in response to a depolarizing current pulse (500-ms duration) in fast-spiking cells sampled from wild-type (current amplitude, 400 pA; top left) and *C6ST-1* mice (300 pA; bottom left). Middle, expanded traces show the second spike evoked by the current pulse. Calibrations were common to the two cells. Right, confocal images showing parvalbumin expression in a fast-spiking cell (arrows) sampled from a mouse. Staining for biocytin (top) and parvalbumin (middle) is shown together with a merged image (bottom). Scale bars represent 10 μm. (**b**) Half width of action potentials. (**c**) Resting membrane potential. *$P < 0.05$ (Student's *t* test) between *C6ST-1* and wild-type mice, and the numbers of fast-spiking cells were 5 (wild-type mice) and 6 (*C6ST-1* mice). Error bars represent s.e.m.

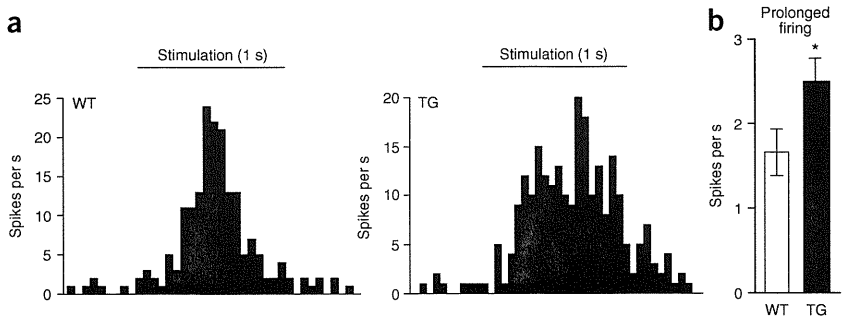

Figure 8 Comparison of visual responsiveness in visual cortical neurons between *C6ST-1* and wild-type mice. (**a**) Examples of post-stimulus time histograms for two cells, each of which was sampled from wild-type (left) and *C6ST-1* mice (right). Bars indicate the time (1 s) of presenting drifting gratings. (**b**) Mean firing rate during a 0.5-s period after the presentation of gratings. Values were calculated after subtraction of spontaneous firing rate. The number of cells was 40 (wild type) and 47 (*C6ST-1*). $*P < 0.05$ (Mann-Whitney test). Error bars represent s.e.m.

of parvalbumin-expressing interneurons[31]. Thus, individual action potentials in mature parvalbumin-expressing interneurons can inhibit their target cells effectively even when the firing frequency is high. In *C6ST-1* transgenic mice, short-term depression may remain stronger and the inhibitory effects of individual action potentials may therefore be weaker when parvalbumin-expressing interneurons fire frequently, as compared with wild-type mice. Thus, it is difficult to predict the overall influence of C6ST-1 overexpression on the inhibitory effects of parvalbumin-expressing interneurons.

To test whether the overexpression of C6ST-1 increased or decreased the inhibitory effects of parvalbumin-expressing interneurons, we examined prolonged firing by extracellular unit recordings from adult visual cortex. It is known that when the inhibitory effects of parvalbumin-expressing interneurons are reduced, visual cortical neurons showed prolonged firing after visual stimulus leave their receptive fields[5,32]. Visual responses were evoked repetitively by stimulation of the contralateral eye with sinusoidal gratings drifting for 1 s. On the whole, the visual responsiveness in *C6ST-1* transgenic mice was very similar to that in wild-type mice. No significant difference was found in orientation selectivity (wild type, $n = 40$ neurons, 0.51 ± 0.068 ; *C6ST-1* transgenic, $n = 47$ neurons, 0.50 ± 0.044; $P > 0.9$), mean firing rate during the optimal stimulation (wild type, $n = 40$ neurons, 7.8 ± 1.5 spikes per s; *C6ST-1* transgenic, $n = 47$ neurons, 6.5 ± 0.71 spikes per s; $P > 0.4$) or spontaneous firing rate (wild type, $n = 40$ neurons, 1.6 ± 0.18 spikes per s; *C6ST-1* transgenic, $n = 47$ neurons, 1.8 ± 0.18 spikes per s; $P > 0.3$) between the two groups. However, we noticed a tendency for prolonged firing after the end of the visual stimulus in *C6ST-1* transgenic mice (**Fig. 8a**), although the degree of prolonged firing seemed weaker than that found in mice deficient for a GABA-synthesizing enzyme[32]. We confirmed this tendency by comparing the mean firing rate during a 0.5-s period after the end of each drifting stimulus between *C6ST-1* transgenic and wild-type mice. The mean firing rate was significantly higher ($P < 0.003$) in *C6ST-1* transgenic than in wild-type mice (**Fig. 8b**). Thus, we conclude that overexpression of C6ST-1 maintains the inhibitory effects of parvalbumin-expressing interneurons in a slightly reduced state until adulthood, mainly as a result of a failure in spike shortening.

DISCUSSION

It has been proposed that there are two classes of molecular brakes that limit plasticity in adulthood[33]. Functional brakes regulate the balance between excitation and inhibition in local circuits. For example, Lynx1, a protein that inhibits nicotinic acetylcholine receptor signaling, restricts plasticity in adulthood through its influence on the balance between excitation and inhibition[34]. On the other hand, structural brakes, such as CSPGs and myelin-related proteins, are thought to limit plasticity by acting as physical barriers based on the mechanism by which they inhibit axonal growth[10,35]. However, our findings suggest an alternative model, in which specific sulfation patterns of chondroitin sulfate chains regulate the maturation of parvalbumin-expressing interneurons through the incorporation of Otx2. Because of the reduced accumulation of Otx2 in parvalbumin-expressing interneurons, *C6ST-1* transgenic mice had a reduced cortical inhibitory tone that did not reach the normal adult level; thus, these mice retained juvenile-like plasticity as adults. Originally, depletion of Otx2 was reported to prevent the initiation of the critical period[5]. Our data suggest that Otx2 also participates in the termination of the critical period. This is not surprising, as the maturation of cortical inhibitory interneurons is crucial for both the onset and termination of the critical period[2]. The onset and termination of the critical period can be accelerated by prematurely enhancing inhibitory transmission[2]. Conversely, reducing intracortical inhibition in adult animals reactivates ocular dominance plasticity after the critical period[36]. The cortical inhibition level has been proposed to cross two thresholds during development[37]. In this model, the critical period is initiated when the inhibition level reaches the first threshold. As development proceeds, the inhibition level increases further and terminates the critical period once it crosses the second threshold. Our data suggest that developmental changes in sulfation patterns of chondroitin sulfate may be required to cross the second threshold, but not the first.

Previous data showed that the number of parvalbumin-immunopositive cells and the intensity of parvalbumin staining were reduced by Otx2 knockdown[5]. We did not find such changes in *C6ST-1* transgenic mice, in spite of the impaired maturation of membrane properties of parvalbumin-expressing interneurons in these mice. Thus, expression levels of parvalbumin do not always correlate with the electrophysiological properties of parvalbumin-expressing interneurons. This idea is supported by the fact that parvalbumin deficiency dose not substantially affect PNN formation and the basic electrophysiological properties of parvalbumin-expressing interneurons[38]. Our results also suggest that the promotion of parvalbumin expression by Otx2 does not require the internalization of Otx2 into the neurons. Instead, a temporal interaction with some signaling molecules on the surface of neurons may be enough to promote parvalbumin expression. How Otx2 regulates parvalbumin-expressing interneuron function is currently unknown. We found that the reduced accumulation of Otx2 prevented the maturation of membrane properties of parvalbumin-expressing interneurons in *C6ST-1* transgenic mice; thus, Otx2 may be required for upregulation of K^+ channels of the K_v3 subfamily underlying brief action potentials[39] and other types of K^+ channels contributing to the hyperpolarization of resting membrane potentials of parvalbumin-expressing interneurons[31].

How the temporal shift of the 4S/6S ratio is regulated remains unknown. We investigated whether reducing cortical inhibition levels, which reactivate the critical period plasticity in adult mice[36],

also reduces the 4S/6S ratio by means of intracortical microperfusion of 3-mercaptopropionic acid (MPA), an inhibitor of GABA synthetic enzyme. However, the 4S/6S ratio in the visual cortex was not affected by MPA perfusion (**Supplementary Fig. 5**). The temporal shift of the 4S/6S ratio may be developmentally programmed and independent or upstream of visual experience or inhibition levels. Expression of several plasticity-associated genes, such as *cartilage link protein-1* (*Crtl1*) and *insulin-like growth factor-1*, is regulated by visual experience[40,41]. On the other hand, expression of myelin-related proteins is independent of visual experience[35]. PNNs formation partially depends on visual experience[10], suggesting that expression of some of these components is regulated by vision. Expression of Crtl1, which is required to stabilize PNNs formation, is downregulated by dark rearing, and *Crtl1*-deficient mice have attenuated PNN formation[40]. Thus, both experience-dependent (for example, Crtl1 expression) and experience-independent (for example, the 4S/6S ratio of chondroitin sulfate chains) factors seem to cooperate for PNN formation. Dysregulation of one of these factors may result in impaired PNN formation and persistent cortical plasticity.

The cellular origin of PNNs has been controversial. The glial origin of PNNs is supported by the fact that they are closely associated with glial processes and that some of their components are synthesized by glial cells[7–9]. In contrast, *in vitro* construction of PNNs in dissociated neuronal culture without glial cells suggests that they originate from neurons[42]. Our findings support the latter possibility, as it was possible to manipulate local PNN formation by parvalbumin-expressing interneuron autonomous elevation of chondroitin 6-sulfation. We also found that C6ST-1 overexpression in non–parvalbumin-expressing interneurons (that is, glial cells and pyramidal neurons) did not affect PNN formation around parvalbumin-expressing interneurons. This may be explained by the fact that the expression patterns of CSPG core protein vary among cell types. For example, brevican is produced in both neurons and glial cells[9], whereas aggrecan seems to be synthesized selectively by parvalbumin-expressing interneurons[43]. Our results indicate that sulfation patterns of CSPGs produced in parvalbumin-expressing interneurons largely contribute to PNN formation. According to a recent model of PNN formation, secreted CSPGs bind to both cell surface hyaluronan and tenascin-R to form massive macromolecules in the pericellular space[8]. Thus, the interaction between CSPGs with other PNN components may depend on the sulfation patterns of chondroitin sulfate. PNNs are very heterogeneous, probably because of differences in the glycan structure of CSPGs[23]. Our data may provide genetic evidence that the heterogeneity of PNNs results, at least in part, from differential sulfation patterns of chondroitin sulfate, which in turn differentially modulate parvalbumin-expressing interneuron function by regulating incorporation of Otx2.

PNN formation is not restricted to the visual cortex and can be found in many brain regions in which Otx2 is not found. Outside the visual cortex, PNNs may facilitate accumulation of other molecules that are secreted from presynaptic terminals. One such candidate is neuronal activity–regulated pentraxin, a secreted synaptic protein that binds to AMPA receptors at excitatory synapses on parvalbumin-expressing interneurons and regulates synaptic plasticity[44]. In the hippocampal neuronal culture, disruption of PNNs with chondroitinase ABC reduces accumulation of neuronal activity–regulated pentraxin on parvalbumin-expressing interneurons[44]. Dysfunction of parvalbumin-expressing interneurons has been implicated in not only cortical plasticity, but also some psychological disorders, such as schizophrenia[45]. It was recently reported that the number of PNNs was reduced in individuals with schizophrenia[46]. Thus, it will be fascinating to assess the contribution of sulfation patterns of chondroitin sulfate in models of these diseases.

METHODS

Methods and any associated references are available in the online version of the paper at http://www.nature.com/natureneuroscience/.

Note: Supplementary information is available on the Nature Neuroscience website.

ACKNOWLEDGMENTS

We thank T. Maruyama and F. Murakami for technical advises on the VEP recordings and *in utero* electroporation, respectively. This work was funded by a Grant-in-Aid for Scientific Research-B 21390025 (to H.K.), grants from the Scientific Research on Innovative Areas (23110003 and 23110004 to H.K. and Y.K.), and a Young Scientists grant (21890286 to S.M.) from Ministry of Education, Culture, Sports, Science & Technology, Japan.

AUTHOR CONTRIBUTIONS

S.M., Y.Y., Y.K. and H.K. designed and performed the research, analyzed the data and wrote the manuscript. S.M. and H.K. conceived the idea. C.T. produced *C6ST-1* transgenic mice.

COMPETING FINANCIAL INTERESTS

The authors declare no competing financial interests.

Published online at http://www.nature.com/natureneuroscience/.
Reprints and permissions information is available online at http://www.nature.com/reprints/index.html.

1. Wiesel, T.N. & Hubel, D.H. Single-cell responses in striate cortex of kittens deprived of vision in one eye. *J. Neurophysiol.* **26**, 1003–1017 (1963).
2. Hensch, T.K. Critical period plasticity in local cortical circuits. *Nat. Rev. Neurosci.* **6**, 877–888 (2005).
3. Gordon, J.A. & Stryker, M.P. Experience-dependent plasticity of binocular responses in the primary visual cortex of the mouse. *J. Neurosci.* **16**, 3274–3286 (1996).
4. Yazaki-Sugiyama, Y., Kang, S., Câteau, H., Fukai, T. & Hensch, T.K. Bidirectional plasticity in fast-spiking GABA circuits by visual experience. *Nature* **462**, 218–221 (2009).
5. Sugiyama, S. *et al.* Experience-dependent transfer of Otx2 homeoprotein into the visual cortex activates postnatal plasticity. *Cell* **134**, 508–520 (2008).
6. Sugahara, K. & Mikami, T. Chondroitin/dermatan sulfate in the central nervous system. *Curr. Opin. Struct. Biol.* **17**, 536–545 (2007).
7. Celio, M.R., Spreafico, R., De Biasi, S. & Vitellaro-Zuccarello, L. Perineuronal nets: past and present. *Trends Neurosci.* **21**, 510–515 (1998).
8. Galtrey, C.M. & Fawcett, J.W. The role of chondroitin sulfate proteoglycans in regeneration and plasticity in the central nervous system. *Brain Res. Rev.* **54**, 1–18 (2007).
9. Carulli, D. *et al.* Composition of perineuronal nets in the adult rat cerebellum and the cellular origin of their components. *J. Comp. Neurol.* **494**, 559–577 (2006).
10. Pizzorusso, T. *et al.* Reactivation of ocular dominance plasticity in the adult visual cortex. *Science* **298**, 1248–1251 (2002).
11. Bradbury, E.J. *et al.* Chondroitinase ABC promotes functional recovery after spinal cord injury. *Nature* **416**, 636–640 (2002).
12. Gama, C.I. *et al.* Sulfation patterns of glycosaminoglycans encode molecular recognition and activity. *Nat. Chem. Biol.* **2**, 467–473 (2006).
13. Mikami, T., Yasunaga, D. & Kitagawa, H. Contactin-1 is a functional receptor for neuroregulatory chondroitin sulfate-E. *J. Biol. Chem.* **284**, 4494–4499 (2009).
14. Nadanaka, S., Ishida, M., Ikegami, M. & Kitagawa, H. Chondroitin 4-*O*-sulfotransferase-1 modulates Wnt-3a signaling through control of E disaccharide expression of chondroitin sulfate. *J. Biol. Chem.* **283**, 27333–27343 (2008).
15. Kitagawa, H., Tsutsumi, K., Tone, Y. & Sugahara, K. Developmental regulation of the sulfation profile of chondroitin sulfate chains in the chicken embryo brain. *J. Biol. Chem.* **272**, 31377–31381 (1997).
16. Properzi, F. *et al.* Chondroitin 6-sulphate synthesis is up-regulated in injured CNS, induced by injury-related cytokines and enhanced in axon-growth inhibitory glia. *Eur. J. Neurosci.* **21**, 378–390 (2005).
17. Fox, K. & Wong, R.O. A comparison of experience-dependent plasticity in the visual and somatosensory systems. *Neuron* **48**, 465–477 (2005).
18. Maeda, N. *et al.* Heterogeneity of the chondroitin sulfate portion of phosphacan/6B4 proteoglycan regulates its binding affinity for pleiotrophin/heparin binding growth-associated molecule. *J. Biol. Chem.* **278**, 35805–35811 (2003).
19. Frenkel, M.Y. & Bear, M.F. How monocular deprivation shifts ocular dominance in visual cortex of young mice. *Neuron* **44**, 917–923 (2004).
20. Godement, P., Salaün, J. & Imbert, M. Prenatal and postnatal development of retinogeniculate and retinocollicular projections in the mouse. *J. Comp. Neurol.* **230**, 552–575 (1984).
21. Sato, M. & Stryker, M.P. Distinctive features of adult ocular dominance plasticity. *J. Neurosci.* **28**, 10278–10286 (2008).
22. Härtig, W., Brauer, K. & Brückner, G. Wisteria floribunda agglutinin-labeled nets surround parvalbumin-containing neurons. *Neuroreport* **3**, 869–872 (1992).

23. Matthews, R.T. *et al.* Aggrecan glycoforms contribute to the molecular heterogeneity of perineuronal nets. *J. Neurosci.* **22**, 7536–7547 (2002).
24. Erisir, A. & Dreusicke, M. Quantitative morphology and postsynaptic targets of thalamocortical axons in critical period and adult ferret visual cortex. *J. Comp. Neurol.* **485**, 11–31 (2005).
25. Marín, O. & Rubenstein, J.L. A long, remarkable journey: tangential migration in the telencephalon. *Nat. Rev. Neurosci.* **2**, 780–790 (2001).
26. Tanaka, D.H. *et al.* Random walk behavior of migrating cortical interneurons in the marginal zone: time-lapse analysis in flat-mount cortex. *J. Neurosci.* **29**, 1300–1311 (2009).
27. Borrell, V., Yoshimura, Y. & Callaway, E.M. Targeted gene delivery to telencephalic inhibitory neurons by directional *in utero* electroporation. *J. Neurosci. Methods* **143**, 151–158 (2005).
28. Kawaguchi, Y. & Kondo, S. Parvalbumin, somatostatin and cholecystokinin as chemical markers for specific GABAergic interneuron types in the rat frontal cortex. *J. Neurocytol.* **31**, 277–287 (2002).
29. Connors, B.W. & Gutnick, M.J. Intrinsic firing patterns of diverse neocortical neurons. *Trends Neurosci.* **13**, 99–104 (1990).
30. Kawaguchi, Y. Physiological subgroups of nonpyramidal cells with specific morphological characteristics in layer II/III of rat frontal cortex. *J. Neurosci.* **15**, 2638–2655 (1995).
31. Goldberg, E.M. *et al.* Rapid developmental maturation of neocortical FS cell intrinsic excitability. *Cereb. Cortex* **21**, 666–682 (2011).
32. Hensch, T.K. *et al.* Local GABA circuit control of experience-dependent plasticity in developing visual cortex. *Science* **282**, 1504–1508 (1998).
33. Bavelier, D., Levi, D.M., Li, R.W., Dan, Y. & Hensch, T.K. Removing brakes on adult brain plasticity: from molecular to behavioral interventions. *J. Neurosci.* **30**, 14964–14971 (2010).
34. Morishita, H., Miwa, J.M., Heintz, N. & Hensch, T.K. Lynx1, a cholinergic brake, limits plasticity in adult visual cortex. *Science* **330**, 1238–1240 (2010).
35. McGee, A.W., Yang, Y., Fischer, Q.S., Daw, N.W. & Strittmatter, S.M. Experience-driven plasticity of visual cortex limited by myelin and Nogo receptor. *Science* **309**, 2222–2226 (2005).
36. Harauzov, A. *et al.* Reducing intracortical inhibition in the adult visual cortex promotes ocular dominance plasticity. *J. Neurosci.* **30**, 361–371 (2010).
37. Jiang, B., Huang, Z.J., Morales, B. & Kirkwood, A. Maturation of GABAergic transmission and the timing of plasticity in visual cortex. *Brain Res. Brain Res. Rev.* **50**, 126–133 (2005).
38. Schwaller, B. *et al.* Parvalbumin deficiency affects network properties resulting in increased susceptibility to epileptic seizures. *Mol. Cell. Neurosci.* **25**, 650–663 (2004).
39. Rudy, B. & McBain, C.J. Kv3 channels: voltage-gated K^+ channels designed for high-frequency repetitive firing. *Trends Neurosci.* **24**, 517–526 (2001).
40. Carulli, D. *et al.* Animals lacking link protein have attenuated perineuronal nets and persistent plasticity. *Brain* **133**, 2331–2347 (2010).
41. Tropea, D. *et al.* Gene expression changes and molecular pathways mediating activity-dependent plasticity in visual cortex. *Nat. Neurosci.* **9**, 660–668 (2006).
42. Miyata, S., Nishimura, Y., Hayashi, N. & Oohira, A. Construction of perineuronal net–like structure by cortical neurons in culture. *Neuroscience* **136**, 95–104 (2005).
43. Lander, C., Zhang, H. & Hockfield, S. Neurons produce a neuronal cell surface–associated chondroitin sulfate proteoglycan. *J. Neurosci.* **18**, 174–183 (1998).
44. Chang, M.C. *et al.* Narp regulates homeostatic scaling of excitatory synapses on parvalbumin-expressing interneurons. *Nat. Neurosci.* **13**, 1090–1097 (2010).
45. Lewis, D.A., Hashimoto, T. & Volk, D.W. Cortical inhibitory neurons and schizophrenia. *Nat. Rev. Neurosci.* **6**, 312–324 (2005).
46. Pantazopoulos, H., Woo, T.U., Lim, M.P., Lange, N. & Berretta, S. Extracellular matrix-glial abnormalities in the amygdala and entorhinal cortex of subjects diagnosed with schizophrenia. *Arch. Gen. Psychiatry* **67**, 155–166 (2010).

ONLINE METHODS

Generation of *C6ST-1* transgenic mice. Full-length human *C6ST-1* cDNA was amplified by reverse transcription PCR (RT-PCR) using a human placenta cDNA library and cloned into the EcoRI site of a pCAG vector, which drives transgene expression using a chicken β-actin promoter and CMV enhancer[47] Plasmid DNA was injected into C57BL6 embryos, which were placed into pseudopregnant females to produce transgenic offspring. Transgenic mice were identified by Southern blot using tail DNA and were mated with C57BL6 wild-type mice. Mice were kept under specific pathogen–free conditions in an environmentally controlled clean room at the Institute of Laboratory Animals, Kobe Pharmaceutical University. All experiments were conducted according to institutional ethics guidelines for animal experiments and safety guidelines for gene manipulation experiments. All animal procedures were approved by the Kobe Pharmaceutical University Committee on Animal Research and Ethics.

Chondroitin sulfate disaccharide composition. Brains were removed and cortical regions were dissected according to a mouse brain atlas and homogenized in cold acetone. The air-dried powder was exhaustively digested with actinase E (Kaken Pharma) at 60 °C for 24 h. The digest was treated with 5% trichloroacetic acid (wt/vol) and the acid-soluble fraction was extracted with diethyl ether. The aqueous phase was neutralized and subjected to gel filtration on a PD-10 column (GE Healthcare). The flow-through fractions were collected, evaporated dry and dissolved in water. An aliquot of the sample was digested with chondroitinase ABC (Seikagaku) at 37 °C for 2 h. The digests were derivatized with a fluorophore, 2-aminobenzamide, and then analyzed by anion-exchange high-performance liquid chromatography (SLC-10A, Shimadzu) on a PA-03 column (YMC). Identification and quantification of the resulting disaccharides were achieved by comparison with chondroitin sulfate–derived authentic unsaturated disaccharides (Seikagaku), as described previously[48].

Monocular deprivation. Monocular deprivation began at P24–26 for critical period mice and P60–P90 in adult mice. The eyelid margins of the right eye were trimmed and sutured under intraperitoneal pentobarbital anesthesia and deprivation continued for 3 or 6 d until the recording. Mice were monitored daily to be sure that the sutured eye remained shut and uninfected. Animals whose eyelids did not fully seal shut were excluded from further experiments.

VEP recordings. Mice were anesthetized with intraperitoneal fentanyl and droperidol and then placed in a stereotaxic frame. A local anesthetic, lidocaine, was administered at pressure points caused by the stereotaxic frame. Body temperature was maintained at about 37 °C. A large portion of the skull overlying the visual cortex was carefully drilled and removed leaving the dura intact. Microelectrodes (300–500 kΩ, Frederick Haer & Co) were inserted into the binocular visual cortex (3 mm lateral of lambda) and advanced 450 μm into the cortex. At this depth, VEPs had their maximal amplitude. Stimuli consisted of full-field sine-wave gratings of 0% and 100% contrast (mean luminance 25 cd m^{-2}, area = 30 × 50 cm), reversing at 1 Hz, and were presented at 0.05 cycles per degree. These stimuli were generated by a VSG4/2 card (Cambridge Research System) and displayed on the face of a monitor (FlexScan T962, Eizo Nanao), which was placed in front of the animal (distance, 28.5 cm). VEPs were elicited by horizontal gratings. VEP amplitude was quantified by measuring the negative peak amplitude of average responses, as described previously[49].

Unit recordings. Adult mice (P60–90) were anesthetized with urethane (1.1 g per kg of body weight, intraperitoneal) supplemented by the sedative chlorprothixene (9 mg per kg of body weight, intramuscular). Unit recordings were conducted from the binocular zone of the primary visual cortex using a tungsten-in glass electrode (3–5 MΩ; Frederick Haer & Co). Cells were recorded across all layers. We analyzed spikes that originated from single neurons using an off-line spike-sorting procedure. Visual stimuli consisted of a full-field drifting sinusoidal grating at a temporal frequency of 2 Hz were applied to the eye contralateral to the recording hemisphere. These stimuli were generated in the Psychophysics Toolbox extensions of MATLAB (Mathworks) and displayed on the face of a monitor (Flexscan T962, Nanao, 160-Hz refresh rate), which was placed in front of the animal (distance, 28.5 cm). To characterize visual responsiveness, we varied the direction of gratings between 0–360° (12 steps) at the spatial frequency between 0.01 and 0.32 (six steps). The orientation selective index was calculated as the ratio of $(R_{pref} - R_{orth})/(R_{pref} + R_{orth})$ at the optimal spatial frequency in each cell, where R_{pref} was the response to the preferred direction and R_{orth} was the mean response of the two directions orthogonal to the preferred direction.

Whole-cell recordings from slice preparations. Coronal slices (300 μm) of primary visual cortex were prepared from mice at P30–34 under deep anesthesia with isoflurane. Slices were cut and recovered for 1 h in oxygenated (95% O_2 and 5% CO_2) artificial cerebrospinal fluid (ACSF) containing 126 mM NaCl, 3 mM KCl, 1.2 mM NaH_2PO_4, 1.3 mM $MgSO_4$, 2.4 mM $CaCl_2$, 26 mM $NaHCO_3$ and 10 mM glucose at 33 °C. Then slices were kept in the ACSF at 24–25 °C. During recording experiments, slices were perfused with ACSF at 24–25 °C. An infrared Olympus DIC microscope with a 40×, 0.8 NA water-immersion lens was used to visualize and target recording electrodes to nonpyramidal neurons located in and near layer 4. Patch pipettes (4–6 MΩ) were filled with an internal solution containing 130 mM potassium gluconate, 8 mM KCl, 1 mM $MgCl_2$, 0.6 mM EGTA, 10 mM HEPES, 3 mM Na^+-ATP, 0.5 mM Na^+-GTP, 10 mM sodium phosphocreatine and 0.3% biocytin (wt/vol) (pH 7.3 adjusted with KOH). Recordings were made using a Multiclamp 700B (Molecular Probes) in the current-clamp mode. For analysis, we selected cells with series resistance less than 20 MΩ and did not compensate the resistance. To assess the membrane properties of recorded cells, we stimulated cells with current pulses (duration, 500 ms) starting from −200 pA and increasing up to 700 pA in 100-pA steps. After recording, the recorded cells were visualized using Alexa Fluor 405–conjugated streptavidin (Molecular Probes).

Immunohistochemistry. Mice were perfused transcardially with phosphate-buffered saline (PBS) followed by 4% paraformaldehyde in PBS (wt/vol). Brains were removed and post-fixed overnight. Coronal sections (30 μm thick) were cut with a vibratome (Leica). Sections were permeabilized with 0.2% Triton X-100 (vol/vol) in PBS, blocked with 2% bovine serum albumin (wt/vol) in PBS, and incubated overnight at 25 °C with primary antibodies to parvalbumin (Swant, mouse monoclonal IgG, 1:5,000), CS56 (Seikagaku, mouse monoclonal IgM, 1:200), Otx2 (Santa Cruz Biotech, goat polyclonal IgG, 1:50 or Abcam, rabbit polyclonal IgG, 1:100), aggrecan (Millipore, rabbit polyclonal IgG, 1:400) or VGluT2 (Millipore, guinea pig polyclonal IgG, 1:500). TRITC-labeled WFA lectin (EY laboratories, 5 μg ml^{-1}) was used for staining perineuronal nets. Sections were incubated with the appropriate Alexa 488/568/647-labeled (Invitrogen) or Cy-5–labeled (Millipore) secondary antibodies for 1 h at 25 °C. After washing with PBS, sections were stained with Hoescht 33342 (2 μg ml^{-1}) to identify cell nuclei. Images were captured with an LSM 710 laser-scanning confocal microscope using a 10× objective (Carl Zeiss). For quantification of the number of WFA-, CS56-, parvalbumin- and Otx2-immunopositive cells, labeled cells were counted in a 1.0 × 1.2 mm area spanning all cortical layers of the primary visual cortex. For three-dimensional reconstruction, we randomly selected PNNs in layer 4 from both wild-type and *C6ST-1* transgenic mice. Images at 0.35-μm steps were acquired using a 63× objective and processed using ZEN software (Carl Zeiss).

***In utero* electroporation.** Ganglionic eminence–directed *in utero* electroporation was performed on E12.5 wild-type mice as described pereviously[32,33]. Briefly, 2–3 μl of a mixture of *pCAG-C6ST1* (1 μg μl^{-1}) and *pCAG-YFP* (1 μg μl^{-1}) plasmid solution was injected into the lateral ventricle using a pulled glass capillary. The head was clasped with a pair electrode (CUY650P2 or CUY650P5; NEPA Gene) at an angle of 30–60° from the horizontal plane. Square electric pulses (30 V for 50 ms, five times in 950-ms intervals) were passed using an electroporator (NEPA21, NEPA Gene).

Immunoblotting. Brains were homogenized in M-PER buffer (Thermo) containing protease inhibitor cocktail (Nacalai) and incubated on ice for 30 min. After centrifugation, protein concentrations of supernatants were determined by BCA assay kit (Thermo). Protein (200 μg) was digested with 5 milliunits of chondroitinase ABC for 2 h at 37 °C. Protein (10 μg) was separated by 5% acrylamide gel electrophoresis, transferred onto PVDF membrane (GE Healthcare), and incubated overnight at 4 °C with primary antibodies to aggrecan (Millipore, rabbit polyclonal IgG, 1:2,000), phosphacan (Developmental Studies Hybridoma Bank, mouse monoclonal IgG, 1:200) or brevican (BD Biosciences, mouse monoclonal IgG, 1:2,000). The blot was incubated with the appropriate horseradish peroxidase–labeled secondary antibodies for 1 h at 25 °C and developed with

doi:10.1038/nn.3023

the ECL detection system (GE Healthcare). The relative abundance of CSPG core proteins was quantified as the density of the band using ImageQuant TL software (GE Healthcare).

Labeling of retinogeniculate axons at dLGN. Mice under pentobarbital anesthesia received intravitreous injections of Alexa Fluor 488– and Alexa Fluor 594–conjugated cholera toxin B subunits (Invitrogen, 2.5 μl of 2 mg ml^{-1} in PBS) into the left and right eyes, respectively, with a 33 G needle. The needle was gently pulled out after being held in place for about 1 min. Mice were perfused at 24 h after injection. Brains were dissected, post-fixed and cut coronally into 100-μm-thick serial sections with a vibratome. Images of the dLGN at the largest cross-section were captured with a LSM 710 laser-scanning confocal microscope.

Quantitative real-time RT-PCR. Total RNA from the retina, dLGN and visual cortex was isolated with the RNeasy mini kit (Qiagen). cDNA was synthesized from 300 ng of total RNA using Moloney murine leukemia virus reverse transcriptase (Promega). We used primer sequences specific for *Otx2* (forward, 5′-CTCGACGTTCTGGAAGCTCT-3′; reverse, 5′-ACTGGCCACTTGTTCCACTC-3′) and *β-actin* (forward, 5′-AGAGGGA AATCGTGCGTGAC-3′; reverse, 5′-CAATAGTGATGCCTGGCCGT-3′). Quantitative real-time RT-PCR was performed using FastStart DNA Master plus SYBR Green I (Roche Applied Science) in a LightCycler ST300 (Roche Applied Science).

Primary cell culture. For primary astrocyte culture, dissociated cerebral cortical cells from P0 wild-type or *C6ST-1* transgenic mice were plated in 10-cm^2 dishes and grown in DMEM (Wako) containing 10% fetal bovine serum (vol/vol) and antibiotics until they reached confluence. Cells were split with trypsin and re-plated in 24-well dishes at a density of 100,000 cells per well (1.9 mm^2) on glass coverslips coated with poly-L-lysine (10 μg ml^{-1}). Medium was changed every 3 d until the cells reach confluence. At that time, the culture consisted mostly of astrocytes. Dissociated neuronal cultures were prepared from cerebral cortices of E18 wild-type or *C6ST-1* transgenic mice and plated onto the astrocyte monolayer at a density of 200,000 cells per well (1.9 mm^2). Cells were maintained up to 18 d in Neurobasal Medium (Gibco) supplemented with 2% B-27 (vol/vol) plus (Miltenyi Biotec), 2 mM glutamax I (Gibco) and antibiotics. Half of the culture medium was replaced every 3–4 d. The cultures were fixed with 4% paraformaldehyde and stained with various antibodies as described above.

Intracortical microperfusion of MPA. Osmotic minipumps (model 1007D, rate = 0.5 μl h^{-1}; Alzet) containing MPA (100 μM in saline) were connected to a cannula (gauge 30) and implanted stereotaxically into the left hemisphere (3 mm lateral to the midline, 2 mm anterior to lambda) of adult mice. MPA was continuously infused for 1 week into the left visual cortex. The left (MPA treated) and the right (control) visual cortex was dissected and homogenized in ice-cold acetone. Chondroitin sulfate disaccharide composition analysis was performed as described above.

Statistical analysis. Statistical significance was determined by using unpaired two-tailed Student's *t* test. Differences were considered to be significant with a *P* value less than 0.05.

47. Niwa, H., Yamamura, K. & Miyazaki, J. Efficient selection for high-expression transfectants with a novel eukaryotic vector. *Gene* **108**, 193–199 (1991).
48. Kitagawa, H., Kinoshita, A. & Sugahara, K. Microanalysis of glycosaminoglycan-derived disaccharides labeled with the fluorophore 2-aminoacridone by capillary electrophoresis and high-performance liquid chromatography. *Anal. Biochem.* **232**, 114–121 (1995).
49. Yoshimura, Y. *et al.* Involvement of T-type Ca^{2+} channels in the potentiation of synaptic and visual responses during the critical period in rat visual cortex. *Eur. J. Neurosci.* **28**, 730–743 (2008).